Alpha radiation dosimetry using Fluorescent Nuclear Track Detectors

Kouwenberg, J. J.M.; de Pooter, J. A.; Wolterbeek, H. T.; Denkova, A. G.; Bos, A. J.J.

DOI
10.1016/j.radmeas.2018.04.009

Publication date
2018

Document Version
Accepted author manuscript

Published in
Radiation Measurements

Alpha Radiation Dosimetry using Fluorescent Nuclear Track Detectors

J.J.M. Kouwenberg, J.A. de Pooter, H.T. Wolterbeek, A.G. Denkova, A.J.J. Bos*

*Corresponding author: Jasper J M Kouwenberg, Radiation, Science & Technology, Delft University of Technology. Mekelweg 15, Delft, the Netherlands. Email: j.j.m.kouwenberg@tudelft.nl

ABSTRACT

To answer the need for better tools for alpha radiation radiobiology and microdosimetry research, a novel irradiation setup based on a honeycomb collimator, in combination with Fluorescent Nuclear Track Detectors (FNTD) for alpha radiation dosimetry and spectroscopy, was introduced. FNTDs are a novel type of small, crystalline detector that can visualize individual alpha particles and simultaneously measure their location, velocity direction and energy with good accuracy. The performance of FNTDs for alpha radiation dosimetry was evaluated for the first time and the results were compared to extrapolation chamber measurements and simulations. The surface dose rate to water of the irradiation setup for two different honeycomb collimators, measured using FNTDs, agreed with the extrapolation chamber measurements within 6%. The simulations underestimated the surface dose rate to water for the first collimator and overestimated the dose for the second collimator, indicating the sensitivity to manufacturing errors in the collimators of this irradiation setup. The dose homogeneity in the setup was measured using radiochromic film and showed variations of less than 5%, making this setup, in combination with the rich information obtained regarding the spatial, angular and energy distributions of the alpha particles, obtained using the FNTDs, ideal for microdosimetry and radiobiology experiments. The accuracy and ease-of-use of FNTDs in addition to the surface or absorbed dose and

fluence of the radiation field indicate that these detectors are prime candidates for research applications in the field of alpha radionuclide therapy.

INTRODUCTION

While interest in alpha radionuclide therapy is still on the rise (Bandekar et al., 2014; Kratochwil et al., 2016; Pandya et al., 2016), the field of alpha radiobiology experiences a severe lack of proper tools. The high LET of alpha radiation leads to more complex DNA damage and repair mechanics (Franken et al., 2011; Prise et al., 1998; Rydberg, 2001) and microdosimetric effects (Huang et al., 2012; Lu and Kiger, 2009; Roeske and Stinchcomb, 1997; Stinchcomb and Roeske, 1992). Precise knowledge of the dose deposited in cells on a macro- and microscale by an alpha radiation field is required to perform these kinds of studies. Accurate alpha radiation (micro-)dosimetry does however remains difficult, partly due to alpha particles being unable to penetrate the walls of most radiation measurement equipment due to their short range (< 100 µm in water). (near-) Wall-less dosimeters like plastic nuclear track detectors (PNTD) (Wertheim et al., 2010), radiochromic film (Aydarous and Ghazaly, 2013), and alpha cameras (Back and Jacobsson, 2010), extrapolation chambers (EC) (Bohm et al., 1991) and simulation (Hamacher and Sgouros, 2001) are therefore commonly applied for alpha dosimetry. A recently introduced new type of detector called fluorescent nuclear track detector (FNTD) has shown to be an excellent alpha spectrometer (Bartz et al., 2013; Kouwenberg et al., 2016) and gamma (Bartz et al., 2011; Sykora and Akselrod, 2010a), neutron (Sykora and Akselrod, 2010a; Sykora et al., 2008, 2009) and ion dosimeter (Greilich et al., 2013; Klimpki et al., 2016; Osinga et al., 2013, 2014; Sawakuchi et al., 2016). FNTDs are small, cheap and reusable and have the ability to measure individual alpha tracks, yielding a rich amount of information regarding the location, track direction, energy and LET of individual particles. This combination has the potential to have the FNTD function simultaneously as alpha spectrometer, dosimeter and, possibly, microdosimeter. This versatile

functionality is unique and can assist the study of radiobiology and microdosimetry for alpha particles greatly.

Radiobiological experiments often require relatively large doses (0.1 – 5 Gy) in large cell cultures (>30 mm diameter dishes) to yield statistically significant result (Franken et al., 2011; Tracy et al., 2015). However, commercially available alpha radiation sources with sufficient activity to induce the required doses within a reasonable timespan (<1 hour) are often much smaller than the used cell cultures, therefore requiring translation of the source to irradiate the whole target volume. In order to address this issue, a novel collimated alpha irradiation setup is introduced to enable uniform irradiation of large areas with a small source.

By combining this novel setup with FNTDs, an experimental setup for alpha radiobiology experiments with extensive knowledge of the radiation field characteristics is presented in order to answer the need for better tools for alpha radiobiology and microdosimetry. Since the FNTDs have not yet been used for alpha dosimetry, this work presents a novel method for alpha radiation dosimetry using these detectors. This method was validated by comparing the FNTD measured surface dose above the irradiation setup, with extrapolation chamber measurements and Monte Carlo simulations and by comparing the FNTD measured angular distribution of the alpha particles, with Monte Carlo calculated distributions.

MATERIALS AND METHODS

Irradiation setup

A setup capable of irradiating large areas with a collimated alpha source was required for future biological experiments. Am-241 sources with high activities usually only cover a relatively small area (95 mm^2 for our source) and therefore require the source to be moved and collimated to evenly irradiate

larger areas. For this research, a honeycomb collimator in combination with linear stages to move the collimated source to preset locations were used to irradiate areas up to 850 mm^2. A 1.1 cm diameter Americium-241 alpha source with an activity of 409.6 kBq ± 1.7% (20-03-1994) was obtained from the Czech Metrological Institute. A 2 μm gold layer covers the estimated 1.3 μm layer of americium oxide to prevent leakage. The source was placed on two digitally controlled linear stages and a lab jack purchased from Optics Focus Instruments Co. Ltd, China. The linear stages were controlled using a motion controller purchased from the same supplier. The source assembly was placed inside a custom-made aluminum frame with a rail above the assembly for sample placement (see Fig. 1). Sample holders for cell cultures and FNTDs were designed in-house and 3D printed using an Ultimaker 2+ with 200 μm layer height and PLA filament.

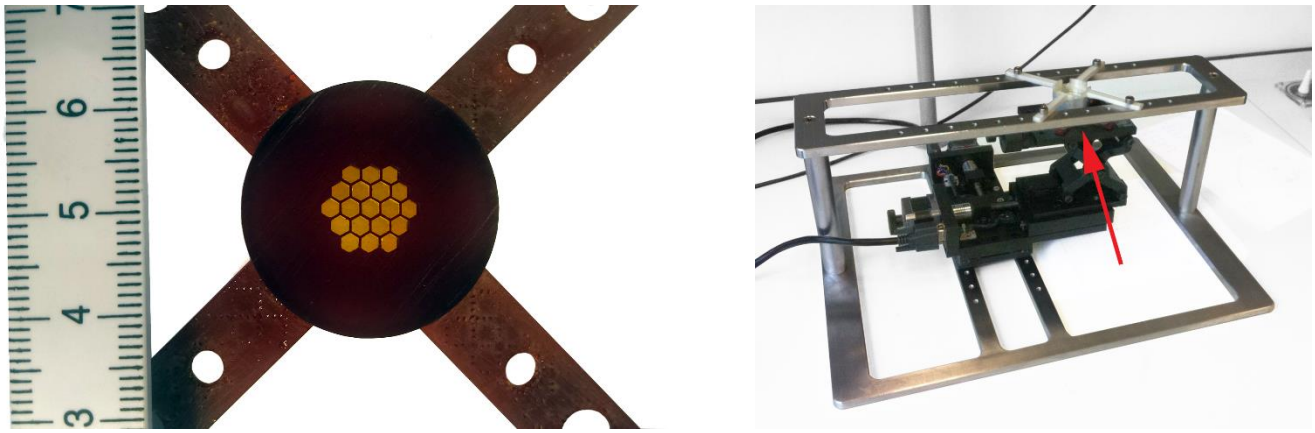

Figure 1: (left) 3D printed honeycomb collimator made using ABS plastic. The gold layer of the source is visible through the honeycomb structure. The given scale is in centimeters. (right) Photo of the aluminum frame with linear stages and a lab jack mounted on the linear stages for source position adjustment. The source (not visible, located at the arrow) was placed on top of the lab jack under the white sample holder.

A collimator with honeycomb structures and wall height of 1800 μm (Figure 1, Figure 3) was designed to restrict the maximum angle of the alpha particles for reliable measurements with both the FNTDs

and the extrapolation chamber. To restrict the maximum angle even more a similar collimator with 2600 µm height was constructed as well. A honeycomb geometry was chosen because it features the same wall thickness throughout the whole geometry (0.2 mm, Figure 2) which leads to a homogeneous alpha radiation induced dose distribution starting from a specific distance above the collimator. This distance was determined using simulation and radiochromic film. The collimators were printed using an EnvisionTEC PERFACTORY® 4 DSP high-resolution printer with 25 µm layer height and ABS filament. A 500 µm thick solid layer was printed on the honeycomb structure for support during printing, but was later removed via sanding. Residual burrs in the honeycomb structure were removed under a microscope using a scalpel. The collimators encapsulated the source and had 4 extending arms which were bolted to the surface of the linear stages. A 400 µm gap between the collimator and the active surface was added to avoid direct contact with the gold protection layer. A sketch of the collimator geometry is given in Figure 2 (left).

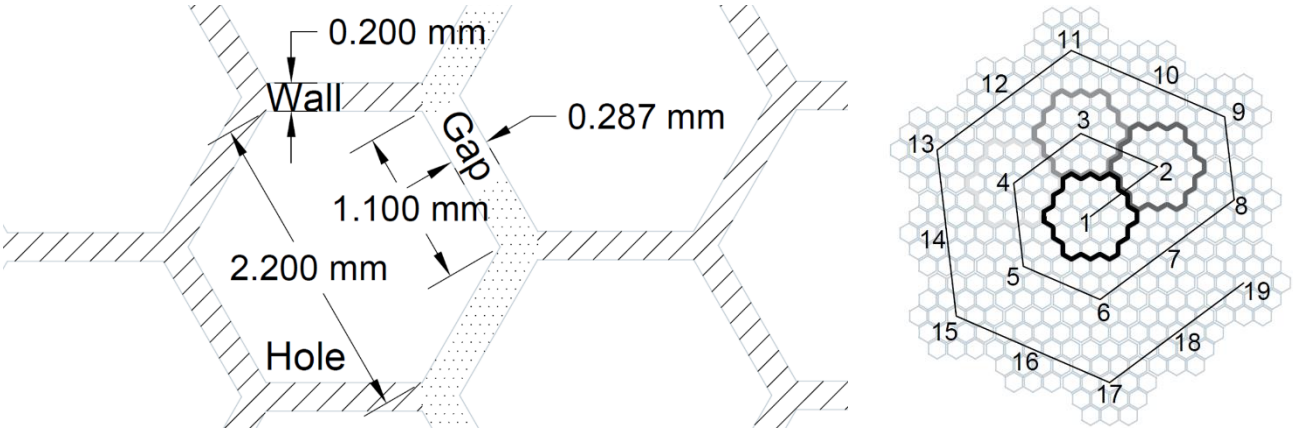

Figure 2: (left) Dimensions of the honeycomb structure as used in the collimators. A single collimator is 5 holes wide. The wall thickness between the holes (dashed) is 0.200 mm. The distance between collimator positions 1 and 2 shown on the right (gap, dotted) is 0.287 mm. A gap size of 0.287 mm instead of the 0.2 mm thickness of the physical walls was found to result in a more even dose distribution. (right) Positioning of the collimator to form an extended honeycomb structure, thereby

creating a large virtual source. The zigzag black line numbered 1, 2, … shows the movement of the collimator center. The dark outlines in the center represent the periphery of the collimator during the first few collimator positions

The positioning in the x,y-plane of the collimated source was done using an in-house build MATLAB interface and RS232 communication with the motion controller. The software placed the collimated source at the indicated positions and the source was halted at each position for a time, chosen based on the desired total dose deposition. Movement between positions 1, 2, … (see Figure 2 (right)) was relatively fast at less than 1 second per transition. By moving the collimated source so that the gap between adjacent collimator positions approximated the wall thickness of the physical collimator, a virtual scalable collimated source could be created (Figure 2, right). It was found that a virtual wall thickness of approximately 0.287 mm, instead of 0.2 mm, led to the most homogeneous dose distribution in radiochromic film, most likely due to small manufacturing errors. For the experiments in this research, only positions 1 through 7 were used. Positions 8 through 19 can be used to create a large field required for biological experiments.

Alignment of the collimated source and sample holder was done by placing 100 μm thick washers between the sample holder arms, so that a deviation of less than 100 μm from the desired distance between the collimator and the sample holder was realized. The deviation was measured at 4 positions on the collimated source: [-12,-12],[12,-12],[12,12],[-12,12] (x,y; mm from center).

Radiochromic Film

In order to find the required distance between the sample and the collimated source to reach a uniform dose distribution, 30 mm diameter slices of Gafchromic^{tm} HD-V2 radiochromic film, kindly provided by PEO Radiation Technology, were irradiated with 60-100 Gy at various heights above each collimator. For each height, the collimator was moved using collimator positions 1 to 7 (Figure 2,

right). The radiochromic film was scanned with a HP Photosmart Premium C310 at 1200 ppi after which the red channel was isolated and converted to optical density using the image-processing software FIJI (Schindelin et al., 2012). The response in optical density, given by eq. (1) in Aydarous et al., of the red channel of the radiochromic film to exposure was shown to be linear in this dose range (Aydarous and Ghazaly, 2013).

FNTD Irradiation and read-out

FNTDs [8 x 4 x 1 (x,y,z) mm^3] were irradiated with approximately 1 Gy above the 1800 and 2600 μm collimators at respectively 5.0 ± 0.1 mm and 7.0 ± 0.1 mm from the active surface. Since the measured area in the FNTDs is small compared to the sizes of the holes of the collimator, the angular distribution of incident alpha particles varied strongly between the irradiation positions.

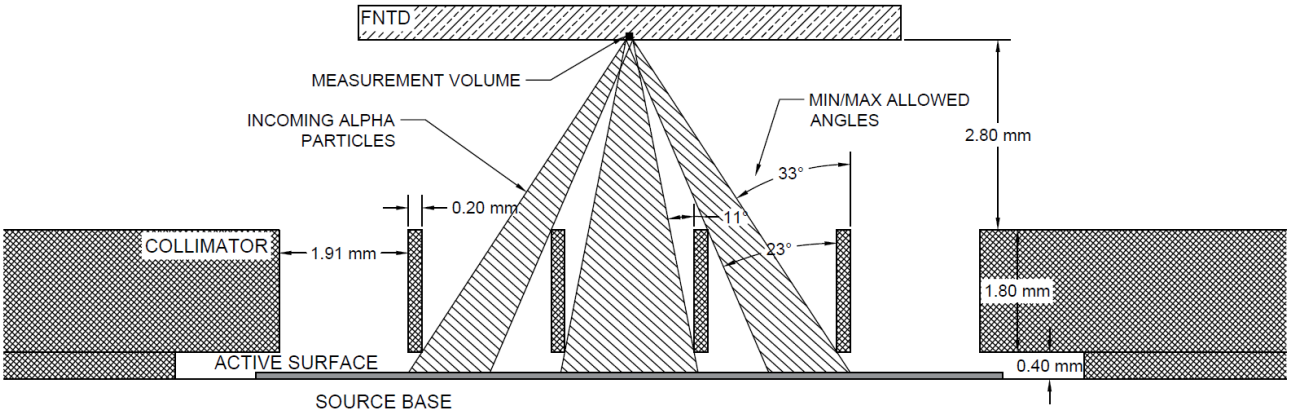

Figure 3: Schematic overview of possible alpha tracks through a 1.8 mm (1800 μm) thick collimator entering the measured area of the FNTD at position 1 (see Fig. 4). A total of 9 irradiations positions were chosen to represent the angular distribution of the whole irradiation field. Note that since a total of 9 positions are used for the irradiation of FNTDs, the collective angular distribution of alpha tracks measured in the FNTDs will yield an angular distribution with less pronounced peaks than found when

looking at individual irradiation positions as shown here.

Therefore, a total of 9 FNTD irradiation positions were chosen based on sampling of the smallest elementary area (Figure 5, left), meaning that the whole collimator could theoretically be built by copying, scaling and rotating this area. In addition, the FNTD irradiation positions were distributed over the whole collimator in order to better represent the spatial variations in the extended radiation field, as illustrated in Figure 5 (right). During each FNTD irradiation, the collimated source was moved to positions 1 to 7 (Figure 2, right). A simplified schematic overview for the first irradiation position above the 1800 μm collimator is given in Figure 3.

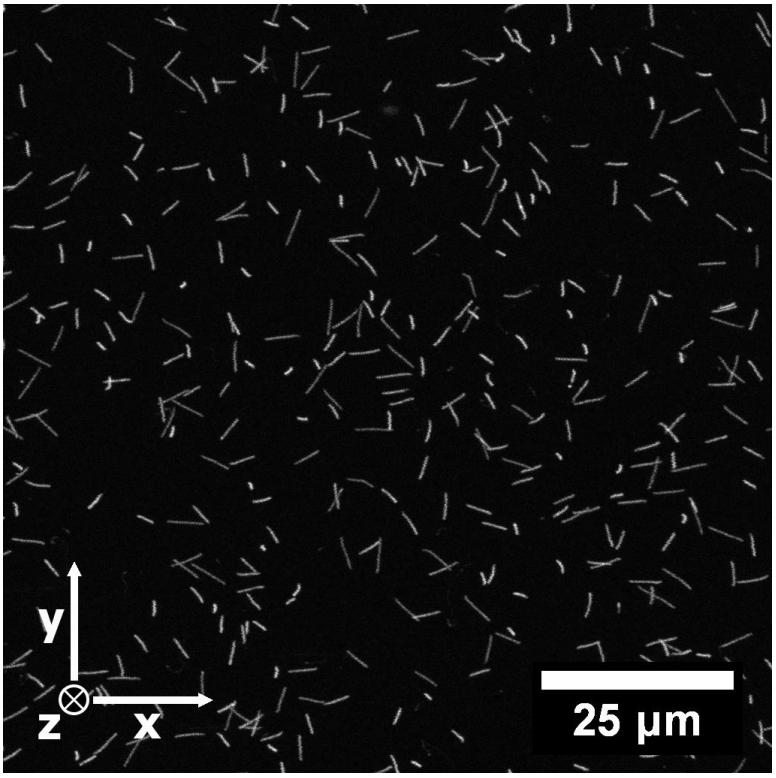

Figure 4: A 2D maximum intensity projection of the fluorescence measured in a 100 x 100 x 12 μm^3 (x,y,z) volume with a confocal laser scanning microscope in a FNTD after irradiation with alpha particles. The apparent length of the tracks is related to the angle of incidence of the alpha particles. Individual tracks were analyzed using in-house build software, yielding the start- and endpoint,

direction, relative scattering, fluorescence intensity and energy for each track.

The center 100 x 100 x 12 μm^3 volumes of FNTDs were read-out using a Leica SP5 confocal laser scanning microscope with Avalanche Photo Diodes (APD) (Figure 4). From the resulting fluorescent image stacks, the tracks induced by passing alpha particles in the measurement volume were reconstructed (Kouwenberg et al., 2016). Track reconstruction yielded for each track l, its path length in the FNTD L_l, initial direction vector given by $x = \chi_l z$ and $y = \gamma_l z$, point of entrance (x_l, y_l, z_l) and corresponding entrance energy (Kouwenberg et al., 2017). The angle of incidence of track l measured in an FNTD was calculated using equation 1:

$$\theta_l = \tan^{-1}\left(\sqrt{\chi_l^2 + \gamma_l^2}\right) \quad (1)$$

Where χ_l and γ_l are the linear slopes between the depth z and respectively the x and y coordinate of track l.

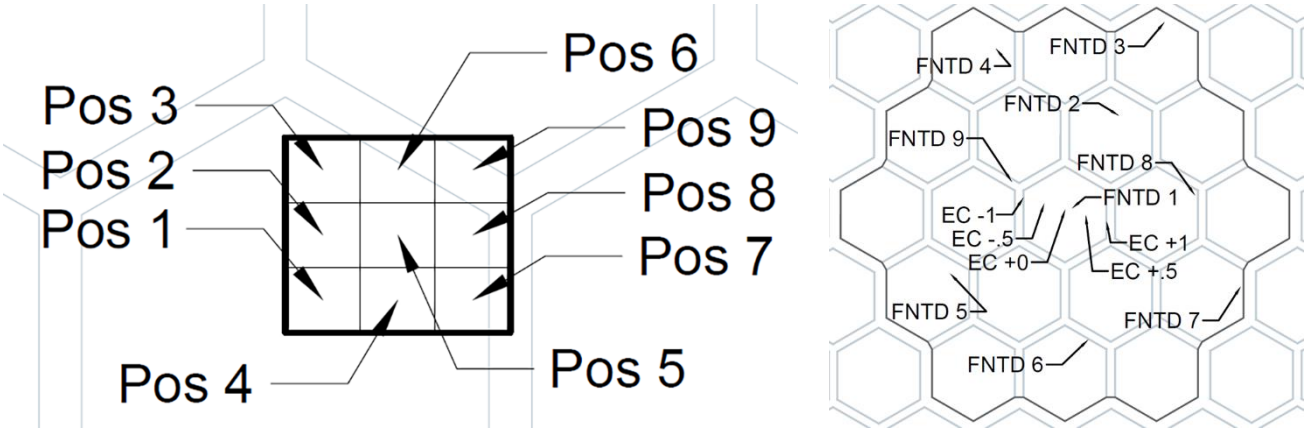

Figure 5: (left) The smallest elementary area (thick outline, 1.05 x 9.1 mm^2) of the collimator and the 9 FNTD sampling positions. (right) Irradiation positions of the centers of the FNTDs divided over the whole collimator, together with the extrapolation chamber (EC) measurement positions. The dark black outline represents the outline of the first collimator position. Multiple collimator positions were

only used during FNTD irradiation.

FNTD Dosimetry

Using the energy and velocity vector of each particle upon entering the FNTD, the water equivalent absorbed dose rate at depth $z = 0$ in the FNTD was calculated via:

$$\dot{D} = \frac{s_{w,Al_2O_3}}{a\,\rho_{Al_2O_3}\,t}\,\frac{N_{total}}{N_{tracked}}\sum_{l=1}^{N_{tracked}}\left.\frac{LET_{Al_2O_3,l}}{\cos(\theta_l)}\right|_{z=0} \tag{2}$$

where $s_{w,Al_2O_3} = 1.408 \pm 2.8\%$ is the stopping power ratio for alpha particles in aluminum oxide and water at 3.7 MeV (Berger et al., 2005; Ziegler, 1999), $N_{tracked}$ is the number of tracked tracks, N_{total} is the number of tracked tracks plus the number of missed tracks, $\rho_{Al_2O_3}$ is the density of aluminum oxide (3790 kg/m^3), t is the irradiation time, a is the measurement surface area, $LET_{Al_2O_3,l}$ is the Linear Energy Transfer of track l in aluminum oxide upon entering the FNTD (derived from the particle energy) (Berger et al., 2005) and the term $1/\cos(\theta_l)$, in which θ_l is the angle of incidence for track l (eq. 1), corrects for the increased dose deposition by tracks not aligned with the z-axis. Since the tracking algorithm colors the reconstructed tracks, tracks missed by the algorithm, and therefore not included in dose calculation, were counted visually. Assuming that the uncertainties in χ_l and γ_l are negligible, the uncertainty of the surface dose estimation can be approximated as:

$$\frac{\sigma_D}{D} \approx \sqrt{\left(\frac{\delta s_{w,Al_2O_3}}{s_{w,Al_2O_3}}\right)^2 + \left(\frac{\delta N_{total}}{N_{total}}\right)^2 + \left(\frac{\delta LET_{Al_2O_3,l}}{\overline{LET_{Al_2O_3,l}}}\right)^2} \tag{3}$$

where the first and second terms in the root are respectively the stopping power ratio and Poisson uncertainties. The last term, the relative uncertainty on LET for track l can be separated into two distinct components. The first component is the uncertainty of the tabulated LET values for alpha particles in matter, which was estimated at 2% for the materials used (Berger et al., 2005; Ziegler,

1999). The second component is the uncertainty of the estimated initial energy of alpha particles entering the FNTD. As shown in an earlier publication (Kouwenberg et al., 2017), almost all particles are in the rising flank of the Bragg peak upon entering the FNTD. No significant bias was observed, but the uncertainty of the measured initial energy distribution was estimated at 200 keV from the difference in measured and simulated alpha particle energy spread of the collimated source. Using the relation between initial energy and LET from NIST's ASTAR, this spread results in a relative uncertainty in the LET of a single track of approximately 3%. The estimates of the initial energies of all individual tracks are fully uncorrelated. Therefore, the contribution of this second component to the total uncertainty of the surface dose must be divided by $\sqrt{N_{total}}$, therefore this component is negligible compared to the Poisson (4.7% for single FNTD, 1.7% for the FNTDs combined) and stopping power uncertainties (2%).

Extrapolation Chamber Dosimetry

The surface dose rate to water for the 1800 (2600 μm) collimator at 5.0 ± 0.1 mm (7.0 ± 0.1 mm) from the active surface was measured using an extrapolation chamber at -1, -0.5, 0, 0.5 and 1 mm from the center to include the spatial variations in the extended radiation field (Figure 5, right). The extrapolation chamber, located at the Dutch Metrology Institute (VSL, Delft, the Netherlands), was similar to the setup used by Bohm et al. (Bohm et al., 1991). The chamber was covered by a 3.5 μm ± 10% polyethylene terephthalate (PE) film with an approximate 20 nm aluminum coating, obtained from Goodfellow Cambridge Ltd., England. By measuring the charge generated in the chamber as function of chamber height z, the absorbed dose rate $\dot{D}$ at $z = 0$ (surface dose) to water was given by eq. (4) (Bohm et al., 1991):

$$\dot{D} = \frac{s_{w,a}}{a\,\rho_{air}}\,\frac{W}{e}\,k_{mylar}\,\frac{d(k_{ad}\,I)}{dz}\bigg|_{z=0} \qquad (4)$$

where $s_{w,a} = 1.17 \pm 2.8\%$ is the stopping power ratio for alpha particles in air and water at 3.7 MeV (average entrance energy) (Berger et al., 2005; Ziegler, 1999), $W/e = 35.08\, J/C \pm 0.8\%$ is the quotient of the mean energy required to produce an ion pair in air (ICRU, 1979), $a = 0.8568\, mm^2 \pm 0.2\%$ is the collector surface area, ρ_{air} is the density of air under reference conditions, $k_{mylar} = 0.923 \pm 1.9\%$ is a correction factor for the increase in stopping power due to the presence of the entrance film (based on simulation and film thickness uncertainty), I is the measured current corrected for saturation effects (Böhm, 1976; Bohm et al., 1991) and k_{ad} is the correction for the deviation of the air density from ρ_0 (for standard pressure p_0 = 101.325 and temperature T_0 = 293.15 K) given by $k_{ad} = p_0 T / p T_0$, where T is the absolute temperature (in K) and p is the air pressure. The charge was measured for 120 (180) s using the 1800 (2600) µm collimator, with both positive and negative polarity, at $z = 0.1, 0.2 \ldots 1.0$ mm. Each measurement was repeated 4 times. $k_{ad} \cdot I$ was fitted to a linear curve using least squares minimization to obtain the slope $d(k_{ad}\, I)/dz$ and its respective uncertainty. FLUKA simulations of the sources within the extrapolation chamber setup showed negligible divergence in dose deposition up to 1 mm chamber heights.

FLUKA Simulation

Simulations of the sources with a 1 mm diameter, 10 µm high air filled cylindrical measurement volume were performed using FLUKA2011 version 2c.3 (Ferrari et al., 2011). The simulation geometry was very similar to Figure 3, but with the FNTD volume replaced by a cylindrical air filled volume. The source, collimator and setup dimensions mentioned in the 'Irradiation setup' section were used for the simulation geometry. The source was modeled as an infinitely thin layer halfway the americium oxide layer, which was modeled using the same density, but with gold atoms instead of americium atoms since higher Z atoms are not available in FLUKA. Each simulation ran for 1E6 particles and was repeated 5 times for uncertainty estimation. The approximate surface dose to water

was calculated by multiplying the obtained dose in air with $s_{w,a}$. No extra dose measurements in the extended irradiation field, created by multiple collimators positions, were performed since simulations showed near-perfect dose uniformity over the whole extended field. The influence of the entrance film in the extrapolation chamber on the stopping power was determined by comparing the surface dose in air with and without aluminized mylar film in front of the air column. The absorbed dose in the mentioned air filled cylindrical measurement volume was obtained using the FLUKA USRBIN routine. A single bin spanning the entire measurement volume was used for the mean absorbed dose determination, while 15 x 15 x 10 μm^3 bins spanning the cylindrical volume were used for dose homogeneity estimation. The angular distribution of particles entering the cylindrical volume was obtained using the USRBDX routine with 120 angle bins, spanning from 0 to 60° after conversion from solid angle to angle of incidence.

RESULTS

Radiochromic film

The dose inhomogeneity in the radiochromic film was found to drop below 5% (standard deviation) from 5.0 ± 0.1 mm (7.0 ± 0.1 mm) for the 1800 (2600 µm) collimator. FLUKA simulations for both collimators showed negligible spatial fluctuations (<0.5%) in surface dose at these heights. Contrast enhanced optical density maps of radiochromic film irradiated at these heights are shown in Figure 6. Intensity profiles along the white lines are given in Figure 7. Relative standard deviations in optical density of 4.4% and 4.6% for respectively the 1800 and 2600 µm collimator were measured in the films. The relative standard deviations in optical density of unirradiated film was below 0.5%. No noise correction was applied to the images. Optical density to absorbed dose conversions were avoided due to the strong LET and angle dependency of the film.

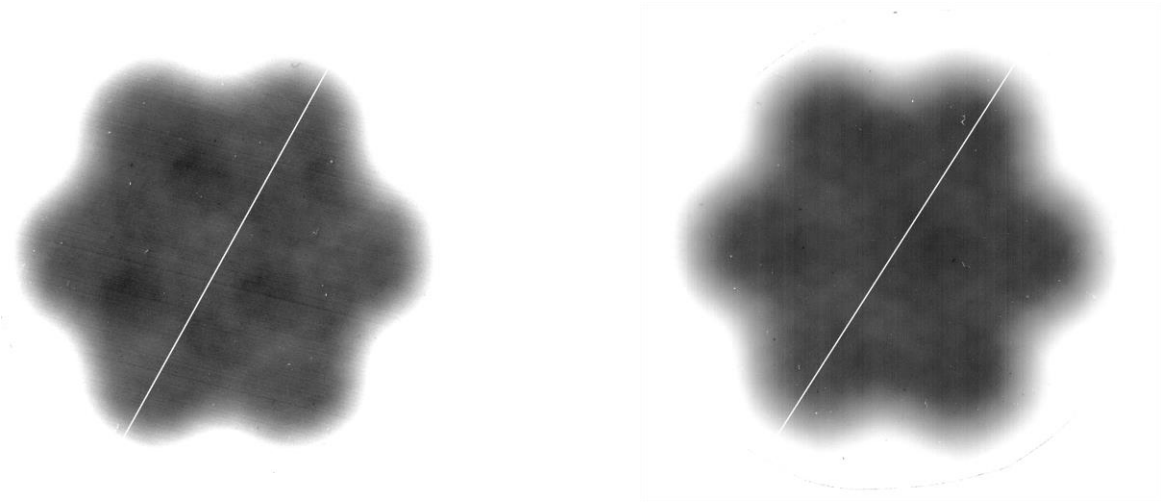

Figure 6: Optical density maps of Gafchromic[tm] HD-V2 film irradiated using the 1800 µm (left) and 2600 µm (right) collimator, contrast enhanced to show the residual unevenness in dose distribution due to the honeycomb structure. Variations in dose distribution were below 5% for both collimators. The white lines are 30 mm long and indicate the position of the intensity profile in Figure 7. White specks are dust particles on the film during scanning.

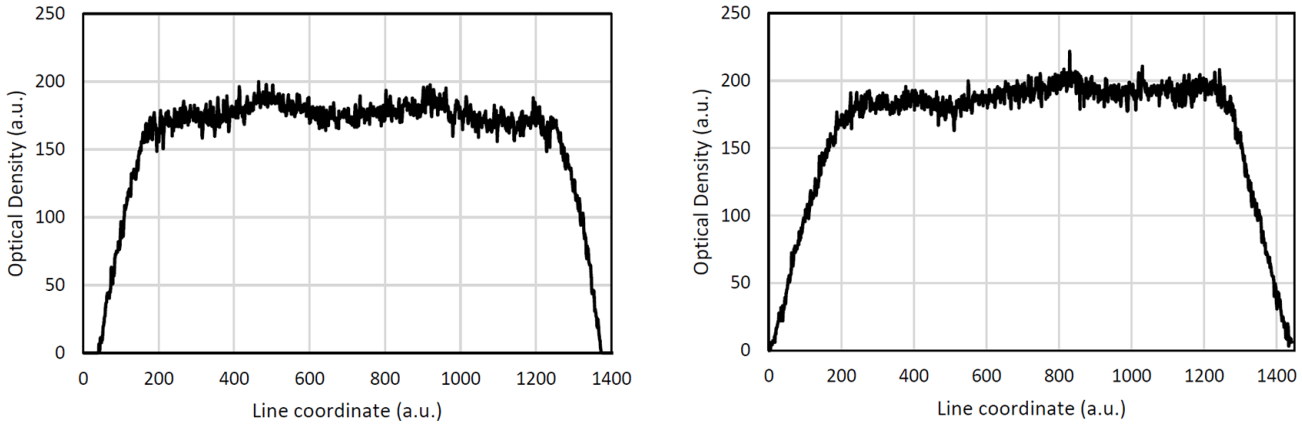

Figure 7: Contrast enhanced optical density maps of Gafchromic[tm] HD-V2 film irradiated using the 1800 µm (left) and 2600 µm (right) collimator.

Angular Distributions

The measured average angular distributions of the irradiated FNTDs for both collimators are shown in Figure 8 together with the corresponding distribution estimated using FLUKA. The missing points near $\theta = 0°$ in the simulated distribution is the result of FLUKA's solid angle binning for angular distributions.

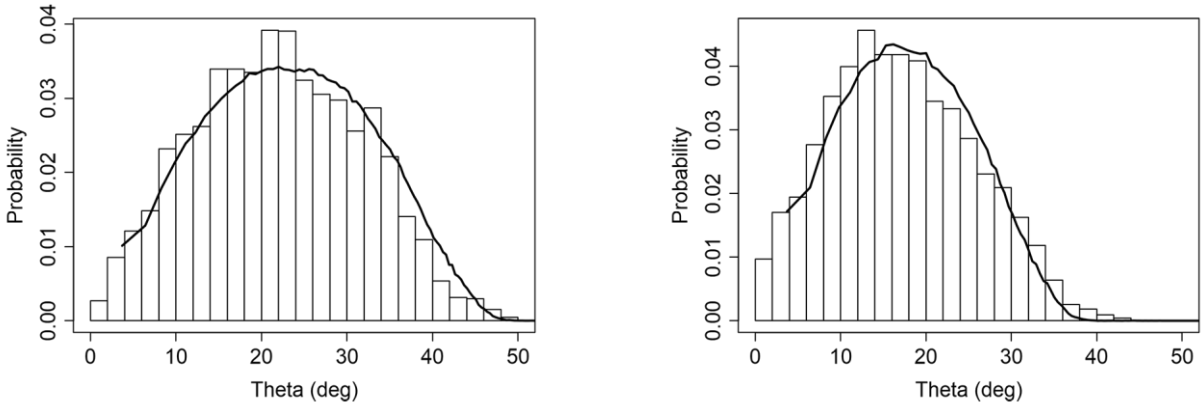

Figure 8: The averaged angular distribution of incoming alpha particles measured using multiple FNTDs irradiated at various positions above the 1800 µm (left) and 2600 µm (right) collimator. The black line represents the distribution obtained using FLUKA.

Dose Measurements

The uncertainties and variance weighted means of the surface dose rates measured using the extrapolation chamber are visualized in Figure 9. The uncertainty in the mean dose rate was given by the uncertainty of the constants given in eq. (4) and the standard deviation of the measurements at the given position. Uncertainties due to fluctuations in measured charge were small compared to others factors (<0.5%). The largest contributions to the uncertainties in the extrapolation chamber measurements were from the stopping power ratio (2.8%) and the mylar film correction (1.9%).

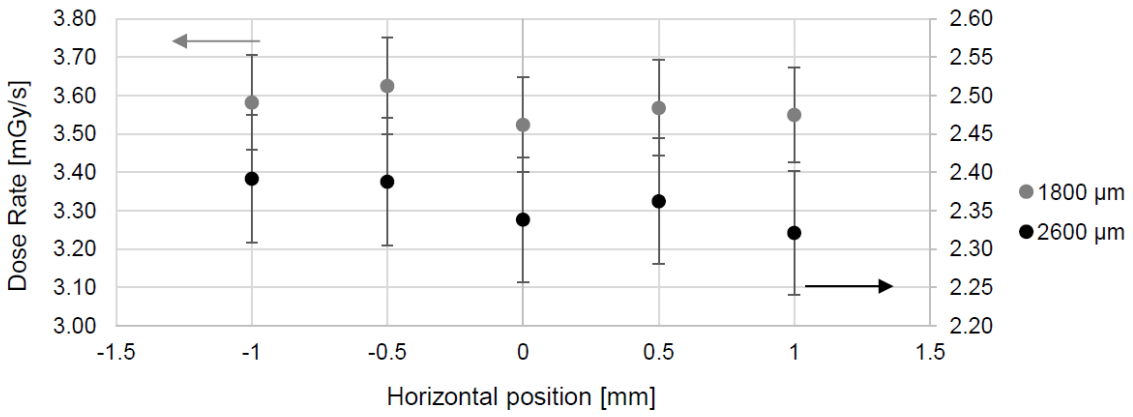

Figure 9: Surface dose rate to water measured using an extrapolation chamber at different horizontal positions above the collimator. Error bars indicate the combined uncertainty, taking into account the uncertainty of the constants given in eq. (4) and the standard deviation of the mean dose rate at the given position.

Out of the 18 irradiated FNTDs, two measurements failed due to poor image quality. A total of 3348 (3251 tracks) were reconstructed while 6 (0) tracks were missed by the algorithm for the 1800 (2600) µm collimator measurements. The measured or estimated surface dose rates based on FNTD, extrapolation chamber and FLUKA data are given together with the respective fluences in Table 1. The uncertainties in the mean dose rates for the FNTD and extrapolation chamber measurements were given by the uncertainty of the constants given in respectively eq. (3) and eq. (4) and the standard deviation of the measurements at the various locations in the radiation field. The latter is related to the dose inhomogeneity in the radiation field, and the inhomogeneity therefore has an effect on the uncertainty of the mean dose rate. Uncertainties in the simulations were a combination of statistical uncertainty from the simulations and the source activity uncertainty. Uncertainties resulting from possible variations in source and collimator geometries due to manufacturing errors were not included in the simulation results.

Table 1: Surface dose rates and fluences as measured or estimated using FNTDs, extrapolation chamber and FLUKA for the two collimators. The uncertainties are given by the standard deviation of the mean dose rate and the uncertainties given in eq. (3) and eq. (4).

	1800 µm Collimator		2600 µm Collimator	
	Dose rate (*mGy/s*)	Fluence (s^{-1} cm^{-2})	Dose rate (*mGy/s*)	Fluence (s^{-1} cm^{-2})
FNTD	3.36 ± 5.9% (5.3%*)	18201 ± 4.4%	2.22 ± 9.0% (5.4%*)	11846 ± 7.8%
Extrapolation Chamber	3.57 ± 3.8% (3.5%*)	-	2.36 ± 3.8% (3.5%*)	-
FLUKA	3.72 ± 5.0%	20744 ± 4.0%	2.06 ± 5.0%	11162 ± 4.0%

** Mean of the relative standard deviations of the individual measurements, excluding the dose inhomogeneity*

DISCUSSION

FNTD measurements underestimated the extrapolation chamber measurements by 5.8% and 5.9% for respectively the 1800 and 2600 µm collimator. While these numbers are within the confidence intervals, the similarity in underestimation for both collimators suggests a systematic cause. A possible cause could be uncertainties in detected locations of the FNTD surfaces in the fluorescence images, leading to an under- or overestimation of the traversed distances of the tracks in the detectors. The maximum reflection intensity of an FNTD in the confocal laser scanning microscope can be used to find the location of the detector surface prior to scanning as shown in an earlier publication (Kouwenberg et al., 2016). The surface location for this set of FNTD scans was refined using a small portion of the tracks and the expected energy from the verified source geometry to allow for comparisons between different imaging methodologies (Kouwenberg et al., 2017). When the source geometry is unknown, detection of the detector surface using only the maximum reflection intensity is, under ideal circumstances, accurate up to 200 nm (Akselrod et al., 2014), which translates to an uncertainty in surface dose rate of approximately 3% for this irradiation setup. Other contributing

factors might include missed or wrongly reconstructed tracks, overestimation of the stopping power ratio for alpha particles in aluminum oxide and water for the FNTD measurements, and possibly an overestimated value for W/e, with the current value for alpha radiation dating back to 1979 for the extrapolation chamber. While the atmospheric conditions were not measured during FNTD irradiations, it is expected that variations in air density did not have a significant impact on the energy, and therefore the stopping power, of the alpha particles upon entering the FNTD due to relatively short path length of the particles through the air. More research is required to find the possible cause of the apparent difference in surface dose rate.

Track overlap was not problematic at the applied dose (~1 Gy), but is expected to interfere with accurate track reconstruction from 2 - 5 Gy. Sykora et al. introduced the power spectrum integral (PSI) approach for high fluence dose estimation in FNTDs (Sykora and Akselrod, 2010b). However, this method suffers from LET dependency and the compatibility with high-LET alpha radiation is unknown. The penetration in the crystal is used to determine the track's initial energy. Therefore, when the source setup is unknown, the dose measurement method described here relies heavily on the correct determination of the detector's surface plane. An automated FNTD reader offers accurate surface plane detection within 200 nm (Akselrod et al., 2014), which translates to an additional 1% uncertainty in LET (3.7 MeV, aluminum oxide). From this it is expected this method is reliable for alpha doses below 2 Gy.

Field inhomogeneity seen in the optical density of the radiochromic films (4.4 - 4.6%) and uncertainties obtained in FNTD measurements (5.9 – 9.0%) were large compared to the uncertainty in mean surface dose rate in the extrapolation chamber measurements (3.8%). The uncertainty of the extrapolation chamber measurements might realistically be higher due to several unknown factors like entrance window flatness and aluminum coating thickness. However, the relatively large difference in uncertainty between the FNTDs and the extrapolation chamber suggest that the inhomogeneity of the

extended radiation field can partly be attributed to small errors in collimator positioning and manufacturing errors at the edge of the collimator. This is especially true for the 2600 µm collimator, where it is expected that the smaller maximum angle of incidence leads to a more localized dose deposition by individual holes in the collimator. Manufacturing errors in the collimator walls will therefore have a larger effect on the dose uniformity. This dose rate location dependency led to the relatively large uncertainty in surface dose rate found using FNTDs. This is reflected by the smaller uncertainties found in measurements of single FNTDs (5.3 – 5.4%). Future studies might benefit from elimination of this location factor and more repeated measurements to better estimate the dose uncertainty of this approach. The angular distributions measured using FNTDs and estimated using FLUKA were in good overall agreement. Meanwhile, it was found that the collimator models in the simulations over- and underestimated the fluence and surface dose rates for the collimators. Possible adjustments to the simulated collimator geometry required to match the surface dose rates found using the extrapolation chamber and the simulations are shown in Table 2. Due to the limited resolution of the 3D printer (25-42 µm) and the additional sanding of the collimator, the indicated possible deviations in wall height and thickness from the design values are not unlikely. Since the simulations both under- and overestimated the surface dose rates, it was considered unlikely that the gold layer thickness differed from the used thickness since the change in attenuation of the alpha particles in the gold layer would have a comparable effect in both collimator simulations.

Table 2: Possible adjustments to the simulated collimator geometries to match the surface dose rates found using simulations and the extrapolation chamber measurements

	1800 µm Collimator		2600 µm Collimator	
	Wall height (µm)	Wall Thickness (µm)	Wall height (µm)	Wall Thickness (µm)
Planned geometry	1800	200	2600	200
Adjusted geometry	1823	206	2516	181

CONCLUSION

FNTD dosimetry was validated with both measurements and simulations. The angular distributions measured using FNTDs were in good overall agreement with simulated distributions. Analysis of the difference between measured and simulated surface dose rates showed that the induced dose rate is very sensitive to small variations in the collimator geometry. Surface dose rate measurement is therefore crucial for setups based on this geometry.

Surface dose rates, measured using FNTDs and extrapolation chamber, were in agreement for both collimator setups. However, uncertainties in surface dose rate due to field inhomogeneity and measurement uncertainties were high for the FNTD approach (5.9 – 9.0%) compared to the extrapolation chamber measurements (3.8%). Since extrapolation chamber measurements were performed in a smaller area than the FNTD measurements, it is expected that similar values could be reached with increased sample sizes, reduction of the dose inhomogeneity in the extended radiation field and further research on the uncertainties and improvement of surface location detection, track reconstruction, energy estimation, geometry and stopping power ratios involved with FNTD alpha dosimetry.

FNTDs nevertheless offer significant advantages. The detectors are small, robust, very cheap, can be read-out multiple times non-destructively and offer rich collection of data, including fluence, angular spectrum and energy. FNTDs can therefore readily be applied for dosimetry of very small (cell nuclei e.g.) volumes and alpha spectroscopy in addition to regular alpha dosimetry. These unique properties make FNTDs strong competitors in the field of alpha radiation dosimetry.

The dose uniformity in larger irradiated areas showed variations of less than 5%, making this setup, in combination with the rich information obtained regarding the spatial, angular and energy distributions of the alpha particles, obtained using the FNTDs, ideal for microdosimetry experiments, irradiation of larger cell cultures and other radiobiology experiments. The individually measured tracks together with the surface dose could be used to estimate the microdosimetric spectra of doses induced in cell nuclei, while the LET and angular spectra find their use in DNA damage and RBE studies. The obtained uncertainties in surface dose are expected to be sufficient for the application in radiobiology.

ACKNOWLEDGEMENTS

The authors are grateful to Dr. Mark Akselrod and Landauer Inc. for kindly donating the FNTDs and to PEO Radiation Technology for donation of the Gafchromic^{tm} HD-V2 radiochromic film. Furthermore, we gratefully acknowledge STW for funding (project number 13577).

REFERENCES

Akselrod, M.S., Fomenko, V.V., Bartz, J.A., Haslett, T.L., 2014. Automatic neutron dosimetry system based on Fluorescent Nuclear Track Detector Technology. *Radiat. Prot. Dosimetry* 161(1), 86–91.

Aydarous, A., Ghazaly, M. El, 2013. Characterization of HD-V2 Gafchromic Film for Measurement of Spatial Dose Distribution from Alpha Particle of 5.5 MeV. *Int. J. Math. Comput. Phys. Electr. Comput. Eng.* 7(7), 1279–1281.

Back, T., Jacobsson, L., 2010. The alpha-Camera: A Quantitative Digital Autoradiography Technique Using a Charge-Coupled Device for Ex Vivo High-Resolution Bioimaging of alpha-Particles. *J. Nucl. Med.* 51(10), 1616–1623. https://doi.org/10.2967/jnumed.110.077578

Bandekar, A., Zhu, C., Jindal, R., Bruchertseifer, F., Morgenstern, A., Sofou, S., 2014. Anti-Prostate-Specific Membrane Antigen Liposomes Loaded with 225Ac for Potential Targeted Antivascular

alpha-Particle Therapy of Cancer. *J. Nucl. Med.* 55(1), 107–114. https://doi.org/10.2967/jnumed.113.125476

Bartz, J.A., Sykora, G.J., Bräuer-Krisch, E., Akselrod, M.S., 2011. Imaging and dosimetry of synchrotron microbeam with aluminum oxide fluorescent detectors. *Radiat. Meas.* 46(12), 1936–1939. https://doi.org/10.1016/j.radmeas.2011.04.003

Bartz, J.A., Zeissler, C.J., Fomenko, V.V., Akselrod, M.S., 2013. An imaging spectrometer based on high resolution microscopy of fluorescent aluminum oxide crystal detectors. *Radiat. Meas.* 56, 273–276. https://doi.org/10.1016/j.radmeas.2013.01.041

Berger, M.J., Coursey, J.S., Zucker, M.A., Chang, J., 2005. ESTAR, PSTAR, and ASTAR: Computer Programs for Calculating Stopping-Power and Range Tables for Electrons, Protons, and Helium Ions (version 1.2.3), National Institute of Standards and Technology, Gaithersburg, MD ,USA.

Bohm, J., Ambrosi, P., Wernli, C., 1991. Measurement of the Depth-Dose Curve of 240Pu Alpha Particles. *Radiat. Prot. Dosimetry* 39(1), 191–194. https://doi.org/10.1017/CBO9781107415324.004

Böhm, J., 1976. Saturation corrections for plane-parallel ionization chambers. *Phys. Med. Biol.* 21(5), 754–759. https://doi.org/10.1088/0031-9155/21/5/004

Ferrari, A., Sala, P.R., Ranft, J., 2011. Fluka: a multi-particle transport code, Stanford Linear Accelerator Center, Stanford, CA, USA.

Franken, N. a P., ten Cate, R., Krawczyk, P.M., Stap, J., Haveman, J., Aten, J., Barendsen, G.W., 2011. Comparison of RBE values of high-LET α-particles for the induction of DNA-DSBs, chromosome aberrations and cell reproductive death. *Radiat. Oncol.* 6(1), 64. https://doi.org/10.1186/1748-717X-6-64

Greilich, S., Osinga, J.M., Niklas, M., Lauer, F.M., Klimpki, G.M., Bestvater, F., Bartz, J.A., Akselrod, M.S., Jäkel, O., 2013. Fluorescent nuclear track detectors as a tool for ion-beam therapy research. *Radiat. Meas.* 56, 267–272. https://doi.org/10.1016/j.radmeas.2013.01.033

Hamacher, K.A., Sgouros, G., 2001. Theoretical estimation of absorbed dose to organs in radioimmunotherapy using radionuclides with multiple unstable daughters. *Med. Phys.* 28(9), 1857–1874. https://doi.org/10.1118/1.1395026

Huang, C.Y., Guatelli, S., Oborn, B.M., Allen, B.J., 2012. Microdosimetry for targeted alpha therapy of cancer. *Comput. Math. Methods Med.* 2012. https://doi.org/10.1155/2012/153212

ICRU, 1979. Average Energy Required to Produce an Ion Pair, International Commission on Radiation Units and Measurements Washington. https://doi.org/10.1017/CBO9781107415324.004

Klimpki, G.M., Mescher, H., Akselrod, M.S., 2016. Fluence-based dosimetry of proton and heavier ion beams using single track detectors. *Phys. Med. Biol.* 61(3), 1021–1040.

Kouwenberg, J.J.M., Ulrich, L., Jäkel, O., Greilich, S., 2016. A 3D feature point tracking method for ion radiation. *Phys. Med. Biol.* 61(11), 4088–4104. https://doi.org/10.1088/0031-9155/61/11/4088

Kouwenberg, J.J.M., Kremers, G.J., Slotman, J.A., Wolterbeek, H.T., Houtmuller, A.B., Denkova, A.G., Bos, A.J.J., 2017. Alpha particle spectroscopy using FNTD and SIM super-resolution microscopy. *J. Microsc.* SUBMITTED.

Kratochwil, C., Bruchertseifer, F., Giesel, F.L., Weis, M., Verburg, F.A., Mottaghy, F., Kopka, K., Apostolidis, C., Haberkorn, U., Morgenstern, A., 2016. 225Ac-PSMA-617 for PSMA-Targeted alpha-Radiation Therapy of Metastatic Castration-Resistant Prostate Cancer. *J. Nucl. Med.* 57(12), 1941–1944. https://doi.org/10.2967/jnumed.116.178673

Lu, X.-Q., Kiger, W.S., 2009. Application of a novel microdosimetry analysis and its radiobiological implication for high-LET radiation. *Radiat. Res.* 171(6), 646–56. https://doi.org/10.1667/RR1612.1

Osinga, J.M., Akselrod, M.S., Herrmann, R., Hable, V., Dollinger, G., Jäkel, O., Greilich, S., 2013. High-accuracy fluence determination in ion beams using fluorescent nuclear track detectors. *Radiat. Meas.* 56, 294–298. https://doi.org/10.1016/j.radmeas.2013.01.035

Osinga, J.M., Brons, S., Bartz, J.A., Akselrod, M.S., Jäkel, O., Greilich, S., 2014. Absorbed dose in ion beams : Comparison of ionization- and fluence-based measurements. *Radiat. Prot. Dosimetry* 161(1–4), 387–392. https://doi.org/10.1093/rpd/ncu004

Pandya, D.N., Hantgan, R., Budzevich, M.M., Kock, N.D., Morse, D.L., Batista, I., Mintz, A., Li, K.C., Wadas, T.J., 2016. Preliminary therapy evaluation of 225Ac-DOTA-c (RGDyK) demonstrates that Cerenkov radiation derived from 225Ac daughter decay can be detected by optical imaging for in vivo tumor visualization. *Theranostics* 6(5), 698–709. https://doi.org/10.7150/thno.14338

Prise, K.M., Ahnström, G., Belli, M., Carlsson, J., Frankenberg, D., Kiefer, J., Löbrich, M., Michael, B.D., Nygren, J., Simone, G., Stenerlöw, B., 1998. A review of dsb induction data for varying quality radiations. *Int. J. Radiat. Biol.* 74(2), 173–184. https://doi.org/10.1080/095530098141564

Roeske, J.C., Stinchcomb, T.G., 1997. Dosimetric framework for therapeutic alpha-particle emitters. *J. Nucl. Med.* 38, 1923–1929.

Rydberg, B., 2001. Radiation-induced DNA damage and chromatin structure. *Acta Oncol. (Madr).* 40(6), 682–5. https://doi.org/10.1080/02841860152619070

Sawakuchi, G.O., Ferreira, F.A., McFadden, C.H., Hallacy, T.M., Granville, D.A., Sahoo, N., Akselrod, M.S., 2016. Nanoscale measurements of proton tracks using fluorescent nuclear track

detectors. *Med. Phys.* 43(5), 2485–2490. https://doi.org/10.1118/1.4947128

Schindelin, J., Arganda-Carreras, I., Frise, E., Kaynig, V., Longair, M., Pietzsch, T., Preibisch, S., Rueden, C., Saalfeld, S., Schmid, B., Tinevez, J., White, D.J., Hartenstein, V., Eliceiri, K., Tomancak, P., Cardona, A., 2012. Fiji: an open-source platform for biological-image analysis. *Nat. Methods* 9(7), 676–682. https://doi.org/10.1038/nmeth.2019

Stinchcomb, T.G., Roeske, J.C., 1992. Analytic microdosimetry for radioimmunotherapeutic alpha emitters. *Med. Phys.* 19(6), 1385–93. https://doi.org/10.1118/1.596770

Sykora, G.J., Salasky, M., Akselrod, M.S., 2008. Properties of novel fluorescent nuclear track detectors for use in passive neutron dosimetry. *Radiat. Meas.* 43(2–6), 1017–1023. https://doi.org/10.1016/j.radmeas.2007.12.038

Sykora, G.J., Akselrod, M.S., Vanhavere, F., 2009. Performance of fluorescence nuclear track detectors in mono-energetic and broad spectrum neutron fields. *Radiat. Meas.* 44(9–10), 988–991. https://doi.org/10.1016/j.radmeas.2009.10.027

Sykora, G.J., Akselrod, M.S., 2010a. Novel fluorescent nuclear track detector technology for mixed neutron-gamma fields. *Radiat. Meas.* 45(3–6), 594–598. https://doi.org/10.1016/j.radmeas.2010.01.037

Sykora, G.J., Akselrod, M.S., 2010b. Spatial frequency analysis of fluorescent nuclear track detectors irradiated in mixed neutron-photon fields. *Radiat. Meas.* 45(10), 1197–1200. https://doi.org/10.1016/j.radmeas.2010.08.022

Tracy, B.L., Stevens, D.L., Goodhead, D.T., Hill, M.A., 2015. Variation in RBE for Survival of V79-4 Cells as a Function of Alpha-Particle (Helium Ion) Energy. *Radiat. Res.* 184(1), 33–45. https://doi.org/10.1667/RR13835.1

Wertheim, D., Gillmore, G., Brown, L., Petford, N., 2010. A new method of imaging particle tracks in solid state nuclear track detectors. *J. Microsc.* 237(1), 1–6. https://doi.org/10.1111/j.1365-2818.2009.03314.x

Ziegler, J.F., 1999. Comments on ICRU Report 49: Stopping Powers and Ranges for Protons and Alpha Particles. *Radiat. Res.* 152, 219–222. https://doi.org/10.1118/1.597176